Chapter 6

Identification of Photons

The charmonium states for which we present results in this dissertation (η_c, η_c', χ_0 and χ_2) are detected by their decay into two photons. We discuss in this chapter the identification of photons using the E835 detector and data acquisition systems. We describe the means by which we determine the energies and positions of particles which deposit energy in the CCAL, and then address the criteria by which we identify a particular energy deposit as being due to a photon.

6.1 CCAL Clustering

Electromagnetic showers initiated by individual electrons or photons striking the CCAL are contained in a small region of the calorimeter, which includes a central block and its eight nearest neighbors. These regions are called clusters. When clusters are isolated from each other (i.e. with centers separated by at least two rings and two wedges) the reconstruction of their position and energy is simple. However, complications arise in instances in which two photons or electrons strike the CCAL in adjacent blocks. In such cases the energy in blocks common to the two clusters must be shared in order that proper energy and position determinations can be made for each incident particle. Further, as $\sqrt{s}$ is increased, it becomes increasingly probable that symmetric decays of π^0s produced in the $\bar{p}p$ interactions result in two photons so close to one another that they are not simply resolvable (i.e. they appear to form a single cluster). It is therefore necessary to have an algorithm which can identify such problem clusters, and which is able to separate, or "split" such clusters appropriately.

In each of the above cases, assignment of position and energy to a cluster is not a simple matter of calculating a center of gravity and a sum over all the blocks in the cluster. The steel partitions among the CCAL blocks form a dead layer which absorbs energy, which must also be accounted for. We will describe in this section the primary algorithm by which clusters in the CCAL are identified and assigned energy and position, and the secondary algorithms which were developed to deal with isolated clusters, clusters which share common blocks, and clusters which must be split into two.

6.1.1 Main Clustering Algorithm

The main clustering algorithm begins identifying all CCAL blocks which contain more energy than their eight nearest neighbors. These blocks, if they contain more than 5 MeV, are identified as "cluster seeds". This seed threshold of 5 MeV is associated with a cluster threshold of 20 MeV. That is, a seed will not be treated as the center of a cluster unless its eight nearest neighbors contain an additional 15 MeV. These thresholds reduce the likelihood that random noise in the calorimeter is incorrectly classified as a cluster.

As the next step, the distance is calculated in block units between each cluster seed in relation to every other cluster seed. The distance D is defined as $\sqrt{\Delta R^2 + \Delta W^2}$, where ΔR is the distance between cluster seeds in ring units, and ΔW the distance in wedge units. This is illustrated in Fig. 6.1. Clusters whose nearest neighbor is farther away than $D_{min} = \sqrt{18}$ are designated as "isolated". Their analysis then proceeds via the isolated cluster routine, which is described in Sec. 6.1.2. If a cluster has one or more neighbors which are as close or closer than D_{min}, it is marked as "non-isolated". The analysis of these clusters proceeds with the cluster energy sharing procedure which is described in Sec. 6.1.3.

Once each cluster has been identified as isolated or non-isolated, a check is performed on all isolated clusters to determine whether they are due to two incident photons from a symmetric π^0 decay, rather than to a single photon. In such cases, as described earlier, the two photons strike within the same 3x3 grid of blocks, and the distribution of energy is such that there is only one discernible local maximum. However, most of these "merged" photon clusters are resolvable because energy is spread over a region larger than the 3x3 square of blocks which surround the single maximum. In order to separate clusters due to single γ or e from these due to "merged" photons, an approximation to the invariant mass may be calculated for a cluster. This "cluster mass" is calculated over the 5x5 square of blocks for all

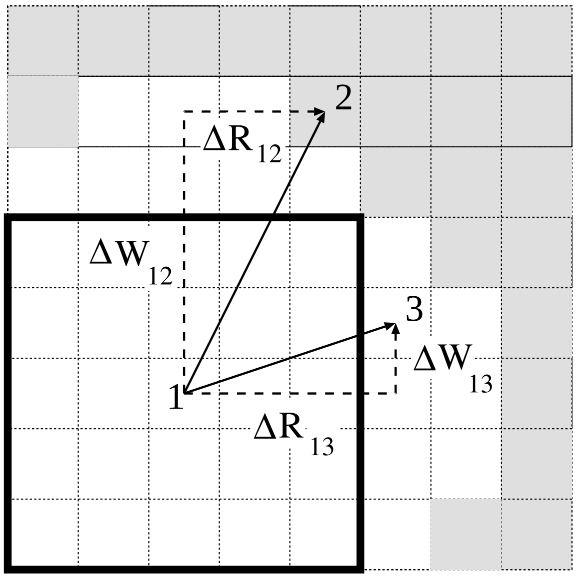

Figure 6.1: Depiction of isolated and non-isolated cluster seeds. Shown is the 5x5 grid around seed #1, and two nearby seeds #2 and #3. Using the definitions in the text, seed #2 has $D_{12} = \sqrt{2^2 + 4^2} = \sqrt{18}$. It, as well as other seeds in shaded blocks, is considered 'isolated' from #1. Seed #3 has $D_{13} = \sqrt{3^2 + 1^2} = \sqrt{10}$, and along with possible seeds in other unshaded blocks, it is not considered 'isolated'.

isolated cluster seeds in the CCAL.

For each block in the 5x5 region around a cluster seed, there are two angles, $\phi(r, w)$ and $\theta(r, w)$, which are measured relative to the $\bar{p}p$ interaction point. We can then calculate an invariant mass for the cluster, using the energy in each block as the fourth component of a four vector directed from the origin to the block center, thus:

$$E_{25} = \Sigma_{5x5}[E(r, w)] \tag{6.1}$$

$$P_x = \Sigma_{5x5}[E(r, w) \times \sin\theta(r, w) \cos\phi(r, w)] \tag{6.2}$$

$$P_y = \Sigma_{5x5}[E(r,w) \times \sin\theta(r,w)\sin\phi(r,w)] \quad (6.3)$$

$$P_z = \Sigma_{5x5}[E(r,w) \times \cos\theta(r,w)] \quad (6.4)$$

$$M_{cluster} = \sqrt{E_{25}^2 - P_x^2 - P_y^2 - P_z^2}. \quad (6.5)$$

If this "cluster mass" is greater than 100 MeV, it is possible that the cluster is due to merged photons from a $\pi^0 \rightarrow \gamma\gamma$ decay. For such clusters, a new second cluster seed is created, in the block with the next highest energy in the cluster. It has been found empirically, by studying clusters due to $J/\psi \rightarrow e^+e^-$ events, that a cluster due to a single incident electron should have cluster mass less than about 100 MeV. In principle, single photons should satisfy the same criterion.

The distribution of cluster masses for neutral clusters in typical run at η_c is shown in Fig. 6.2, where it is compared to the cluster mass distribution for electrons from $J/\psi \rightarrow e^+e^-$. Clusters whose mass is found to be greater than 100 MeV are analyzed in the "cluster splitting algorithm" which is described in Sec. 6.1.4.

6.1.2 Isolated Cluster Analysis

The basic idea behind the isolated cluster energy and position evaluation is common to all experiments which use segmented calorimeters. To first order, the energy E_0 of a cluster is determined by summing the energies in each of the 3x3 set of blocks, and the positions (R_0, W_0) in block units are calculated using simple weighted averages:

$$E_0 = \sum_{i=1}^{9} E_i, \quad R_0 = \frac{\sum_{i=1}^{9} E_i \Delta R_i}{E_0}, \quad W_0 = \frac{\sum_{i=1}^{9} E_i \Delta W_i}{E_0}. \quad (6.6)$$

Here, the ΔR_i and ΔW_i are the positions of each block in the 3x3 grid relative to the central block, i.e. $\Delta R_i, \Delta W_i \in (-1, 0, 1)$. Thus, R_0 and W_0 range from -.5 to

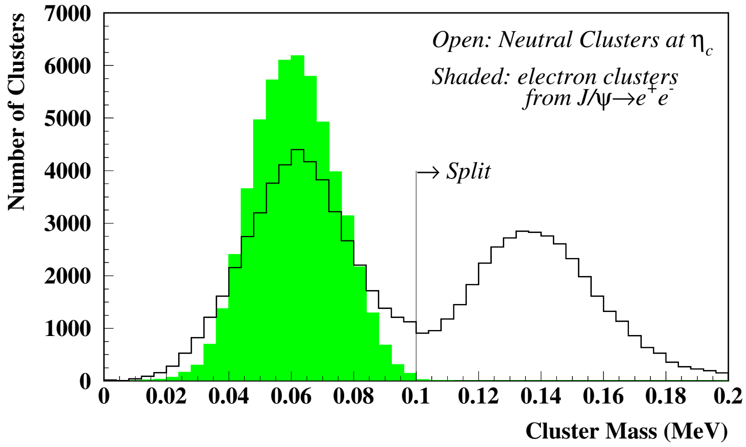

Figure 6.2: Comparison of cluster masses for electrons (shaded) from $J/\psi \to e^+e^-$ and for neutral clusters at η_c (open). The neutral cluster sample shows evidence for "merged" γ's due to symmetric π^0 decay.

+.5, with $(R_0, W_0) = (0{,}0)$ corresponding to the center for the central block.

Electromagnetic showers in typical calorimeter materials such as lead glass are characterized by a narrow shower deposit and long exponential tails. Thus the first order centroids R_0 and W_0 are dominated by the large energy deposit in the central block. The true position of the shower, then, must be obtained through corrections to the centroid which depend on a formula for the transverse shower development in the lead glass, whose parameters must be determined empirically for any particular calorimeter. In terms of the first order cluster centroids R_0 and W_0, the formula for the true position R and W can be written in terms of four parameters, α_R, λ_{AR}, β_R and λ_{BR}:

$$R = (\alpha_R \times (1 - e^{|R_0|/\lambda_{AR}}) + \beta_R \times (1 - e^{|R_0|/\lambda_{BR}})) \tag{6.7}$$

$$W = (\alpha_W \times (1 - e^{|W_0|/\lambda_{AW}}) + \beta_W \times (1 - e^{|W_0|/\lambda_{BW}})). \quad (6.8)$$

In preparation for E760, three CCAL wedges were taken to the Brookhaven National Laboratory to be tested using a 5 GeV electron beam. [46] The actual position of electrons incident upon the blocks in this test setup was recorded by wire chambers. Parameters for Eqs. 6.8 were determined empirically by comparison of the actual beam particle position to the first order calculation of cluster centroids.

As stated earlier, the presence of steel in the interstitial spaces must be corrected for in order to obtain the correct energy for a cluster. This correction has been parameterized in terms of the positions R' and W', which are measured from the edges of the block, i.e. $R' = R - R_{center}$ and $W' = W - W_{center}$:

$$E = E_0 / \left[(1 - \zeta_R * e^{-|R'|/\xi_R})(1 - \zeta_{AW} * e^{-|W'|/\xi_{AW}} - \zeta_{BW} * e^{-|W'|/\xi_{BW}}) \right]. \quad (6.9)$$

The parameterization in the ring direction is different from that in the wedge direction because of the different amount of steel separating rings and wedges (see Sec. 4.4.3). Furthermore, correction due to inter-ring material, because of the staggering of blocks (see Fig. 4.18), is parameterized differently depending upon whether the position R lies in the upstream or downstream half of the ring. ($\zeta_R = \zeta_{dR}$ or ζ_{uR}; $\xi_R = \xi_{dR}$ or ξ_{uR})

All the parameters discussed in this section were determined during the electron beam tests at BNL. Their values appear in Table 6.1.

Table 6.1: Parameters for correction of initial ring and wedge position and energy estimates.

Parameter	Value	Parameter	Value	Parameter	Value	Parameter	Value
α_R	0.260	α_W	0.314	ζ_{dR}	0.061	ζ_{AW}	0.147
λ_{AR}	0.032	λ_{AW}	0.040	ξ_{dR}	0.136	ξ_{AW}	0.020
β_R	0.257	β_W	0.197	ζ_{uR}	0.086	ζ_{BW}	0.159
λ_{BR}	0.186	λ_{BW}	0.172	ξ_{uR}	0.051	ξ_{BW}	0.078

6.1.3 Non-Isolated Cluster Analysis

In the case of two clusters ($j = 1, 2$) which are close enough so that sharing energy between clusters needs to be considered, initial cluster energies and positions are calculated using weighted energies in each block of the cluster. Thus, Eqs. 6.6 are replaced by:

$$E_{0j} = \sum_{i=1}^{9} \eta_{ij} E_i, \quad R_{0j} = \frac{\sum_{i=1}^{9} \eta_{ij} E_i \Delta R_{ij}}{E_{0j}}, \quad W_{0j} = \frac{\sum_{i=1}^{9} \eta_{ij} E_i \Delta W_{ij}}{E_{0j}}. \tag{6.10}$$

i.e. the formulae used are the same as if an energy $\eta_{ij} E_i$ was deposited in the ith block, rather than the measured energy E_i. The weights η_{ij} are dependent upon the position of the ith block from the centroid of the jth cluster, (j = only 1 or 2) and are normalized so that $\eta_{i1} + \eta_{i2} = 1$. They are calculated according to the following iterative procedure.

Initially, the weights η_{ij} are set to 1 for each block shared between the two clusters. (so the normalization rule does not hold in the first iteration) Shared blocks are those which lie within the 5x5 region of both clusters. For other blocks, the η_{ij} is set to 1 for the cluster which is closer. E_{0j}, R_{0j} and W_{0j} are then calculated according to these weights, as a first approximation.

After defining the distance $D_{ij} \equiv \sqrt{(\Delta R_{ij})^2 + (\Delta W_{ij})^2}$ between the ith block and the centroid of the jth cluster in block units, the η_{ij} are defined:

1. If both D_{i1} and D_{i2} are $\leq \sqrt{3.5}$ blocks, the weights η_{ij} take the following form:

$$\eta_{i1} = \frac{E_1 e^{-(\Delta_1/0.17}}{E_1 e^{-\Delta_1/0.17} + E_2 e^{-\Delta_2/0.17}} \tag{6.11}$$

$$\eta_{i2} = \frac{E_2 e^{-\Delta_2/0.17}}{E_1 e^{-\Delta_1/0.17} + E_2 e^{-\Delta_2/0.17}}, \tag{6.12}$$

   with $\Delta_1 \equiv |\Delta R_{i1}| + |\Delta W_{i1}|$ and $\Delta_2 \equiv |\Delta R_{i2}| + |\Delta W_{i2}|$. The 0.17 in the exponents is the characteristic transverse shower decay length in block units, which was empirically determined.

2. If, however, $D_{i1} \leq D_{i2}$ and $D_{i1} \leq \sqrt{4.5}$ blocks, then

$$\eta_{i1} = 1 \quad \text{and} \quad \eta_{i2} = 0. \tag{6.13}$$

   and vice versa.

3. Finally, if $D_{i1} \geq \sqrt{4.5}$ blocks and $D_{i2} \geq \sqrt{4.5}$ blocks, then

$$\eta_{i1} = 0 \quad \text{and} \quad \eta_{i2} = 0. \tag{6.14}$$

Given these weights η_{ij}, new cluster centroid positions and energy estimates are calculated according to Eq. 6.10. If the change in either cluster's energy (from the previous iteration) is greater than 30 MeV, or if the change in either cluster's position is greater than .005 blocks in either dimension, another iteration is performed. This procedure usually converges after 2 or 3 iterations.

6.1.4 Cluster Splitting Analysis

In order to split clusters whose cluster mass is over 100 MeV, a choice must be made as to the locations of the "daughter" cluster seeds. In our algorithm the initial position of one seed is the center of the block which represents the "parent" cluster maximum. The second seed is placed at the center of the next highest energy block in the "parent" cluster - which must be one of the eight nearest neighbors of the first seed.

Once the seeds have been chosen, energy and position corrections for the two "daughter" clusters uses an iterative algorithm nearly identical to that for the energy sharing procedure (Sec. 6.1.3). The only differences between the two routines is that:

- The central maximum is not used in determining initial positions and energies.
- The limit of $\sqrt{4.5}$ blocks presented in items 2 and 3 of the energy sharing procedure (Eq. 6.13 and 6.14) is changed to $\sqrt{8.5}$ blocks.

6.2 Photon Identification

The identification of a CCAL cluster as a photon is based on two simple criteria:

1. The cluster must not be associated with a charged track; that is, the cluster must have no corresponding "track" in the scintillator hodoscopes. Specifically, there can be no coincidence in $H1 \cdot H2'$. Recall that an $H1 \cdot$H2$'$ coincidence removes an event at the trigger level through the Neutral Veto.

2. It must have a cluster mass of less than 100 MeV.

6.2.1 Possible Misidentification of γ's

Given the above conditions for calling a cluster a photon, there are two possible phenomena which in principle can give rise to a false identification.

1. *An electron which did not fire the Neutral Veto* This phenomenon should be rare, but must be considered. The CCAL responds the same way to a single photon as it does a single electron. Shower shapes in lead glass are known to be very similar whether the incident particle is a photon or an electron. Without information from the charged tracking, there is no means of distinguishing between an electron cluster and a photon cluster. In an e^+e^- event, though, the identification of the second electron can help remove this ambiguity.

2. *A π^0 which decays symmetrically, such that the showers of its two photons form a single cluster in the CCAL.* This background is taken care of in large part by an evaluation of the cluster mass, which was introduced in the previous section. If $M_{cl} \geq 100$ MeV, (see Fig. 6.2) the cluster is split using the algorithm described in Sec. 6.1.4. If an event contains a cluster which has been split in this manner, it is removed from the $\gamma\gamma$ data sample.

   It should be noted that there is a small chance that some of the γ candidate clusters arise from a π^0 whose photons have merged, but which gave a cluster mass $M_{cl} \leq 100$ MeV (and was therefore not split). This might suggest lowering the cut below 100 MeV. It was found, however, that changing the value of the splitting threshold from $M_{cl} \leq 100$ MeV does not improve the signal-to-background ratio at η_c.

Table 6.2: Estimated thicknesses (in radiation lengths) of the E835 inner detectors.

Detector		Material	thickness (mm) at normal incidence	Radiation Lengths	Total
Hodoscope	$H1$	scintillator	2	0.47%	0.47%
Straws	$SC1$	Mylar	0.3	0.1%	0.57%
Hodoscope	$H2'$	scintillator	4	0.94%	1.51%
Silicon	SI	various	-	$2.0 - 4.5\%$	$3.5 - 6.0\%$
Straws	$SC2$	Mylar	0.3	0.1%	$3.6 - 6.1\%$
Fiber	SF	various	-	$\sim 1\%$	$\sim 4.6 - 6.1\%$
Hodoscope	$H2$	scintillator	4	0.94%	$\sim 5.6 - 7.1\%$
Čerenkov	$\check{C}$	various	-	$\sim 2.5\%$	$\sim 8.1 - 9.6\%$

6.2.2 Inefficiency due to γ conversions

Real $\gamma\gamma$ events may not be identified as such if one or the other photon converts in material between the interaction region and the CCAL. An appropriate set of cuts can be made, however, so that these events are retained. This requires a study of such conversion events. We can then estimate the inefficiency, if any, due to photon conversions. For reference, we present in Table 6.2 the estimated thickness (for normal incidence) for all inner detectors.

Beampipe conversions and in $H1$

If photon in a $\gamma\gamma$ event converts in the beampipe, (rad length $\lesssim 1\%$) the event will always be lost. Since the beam pipe lies inside the radius of $H1$, a beampipe conversion will result in a charged track in the hodoscopes, and thus the neutral veto will be fired. It is also possible that a γ conversion which occurs in $H1$ itself can fire the neutral veto. If the conversion occurs early enough in the scintillator thickness, it is possible that the resulting "double track" will give a sufficiently large pulse height in $H1$ that, with the corresponding signal in $H2'$, will fire the neutral veto. These events will be lost as well, and being indistinguishable from beam pipe conversions.

The probability of a these two types of conversions was measured in E760 to be ~1.1% per photon, and this value has been confirmed in E835 data. [47]

Conversions after $H1$

Conversions which occur after $H1$ will not fire the neutral veto, and thus make up part of the neutral trigger data set. These conversions may occur in any of the inner detectors which lie outside of $H1$: $SC1$, $H2'$, SIL, $SC2$, SF or $H2$ (See Fig. 4.12). The Straws ($SC1$ and $SC2$) and the Scintillating Fiber Tracker (SF) do not comprise much material at all, ($\sim$ 1.2% of a rad length; see Table 6.2) and therefore are not expected to contribute much in the way of conversions, and are not considered here. However, the Hodoscopes (each $\sim$ 1%) and Silicon barrel ($\sim$ 2.0 – 4.5%) can be expected to cause conversions, and this possibility has been examined.

Photons which convert after H1 can be identified by their signal in the hodoscopes, or in the Čerenkov detector. The pulse height spectra (in equivalent MIP units) for hodoscopes $H1$, $H2'$ and $H2$, and for the Čerenkov detector, are shown in Fig. 6.3-6.6, for events recorded in the J/ψ and $^1P_1$ regions. In these figures, the shaded histogram shows the pulse height for events in the neutral set - i.e. "gold gg" events taken at the $^1P_1$. The unshaded histogram shows the same for events

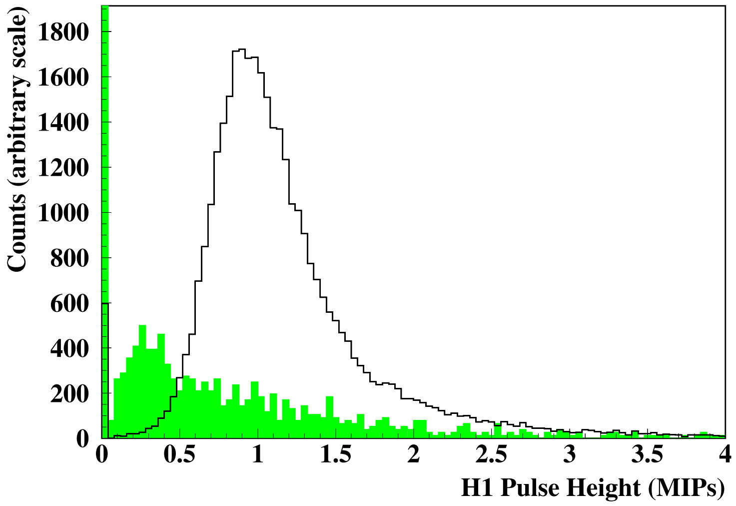

Figure 6.3: Pulse height spectra (in MIP units) from $H1$ for electrons (open histogram) and photons (shaded histogram).

from the charged trigger - e^+e^- events taken at J/ψ. The shaded and open pulse height spectra have been arbitrarily normalized, in order to make comparison of the shapes of the two distributions easier.

In the $H1$ spectrum (Fig. 6.3) there is no identifiable enhancement for neutral events in the 1.5 - 3.0 MIP region. This indicates that the fraction of events representing γ's which converted prior to incidence on $H1$ is essentially nil as expected. A clear, though small, enhancement in the $H2'$ pulse height spectrum in the 1.5-3.0 MIP region is, however, seen after we have greatly magnified the count scale. (See Fig. 6.4) This indicates that the fraction of possible conversions which occur inside the radius of $H2'$ is quite small. In contrast, "double" tracks (pulse heights in the range 1.5-3.0 units) are prominent in the $H2$ and Čerenkov plots. (Figs. 6.5 and

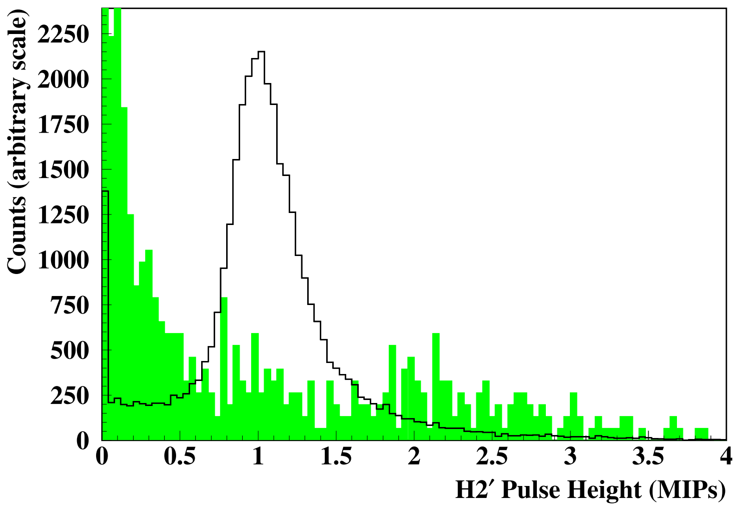

Figure 6.4: Pulse height spectra (in MIP units) from $H2'$ for electrons (open histogram) and photons (shaded histogram).

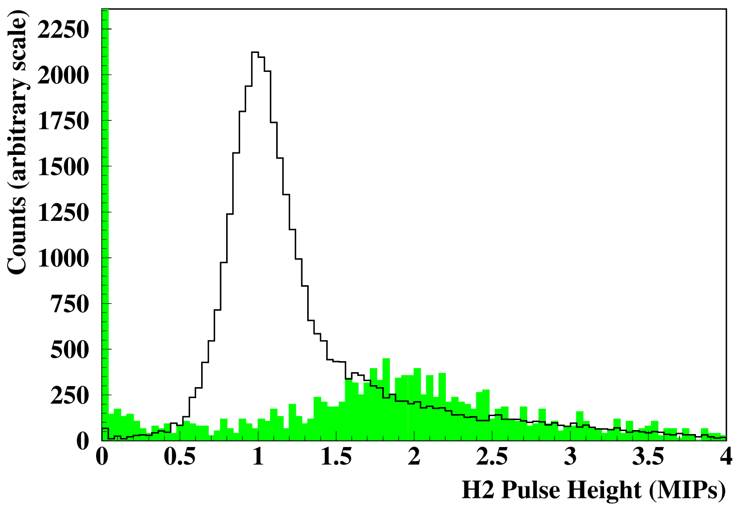

Figure 6.5: Pulse height spectra (in MIP units) from $H2$ for electrons (open histogram) and photons (shaded histogram).

6.6) This observation is consistent with the hypothesis (see Sec. 4.4.1) that most of the conversions we detect occur in the silicon barrel, which lies just inside $H2$.

Do we lose these events?

The primary concern we have regarding conversions is whether or not we unwittingly remove them from our event sample, due to the cuts we make. As outlined in the next chapter, the only cut which we use to remove charged final state events is a cut on the pulse heights in $H1$ and $H2'$. We have shown that most conversions occur beyond $H2'$. Thus most events containing γ conversions should pass cuts on $H1$ and $H2'$ pulse heights. In order to show that this is indeed the case, we have studied the effect of applying the $H1$ and $H2'$ cuts to events containing conversions.

For the purpose of this study, we have defined a converted photon as a CCAL cluster having pulse heights in corresponding elements of both $H2$ and Č between 1.5 and 3 MIP units. We have examined events in the η_c, $^1P_1$ and η_c' regions, comparing the total number of 2-cluster events in the "gold gg" trigger sample to the number of conversion candidates as defined above. We also list the number of these candidates which are removed due to the cuts on the pulse heights in $H1$ and $H2'$. The number of conversions, $\sim 8\%$ on average, is somewhat large, but it is of no consequence, since the number events which we remove is a very small proportion of the total number of $\gamma\gamma$ candidate events ($\leq 0.6\%$).

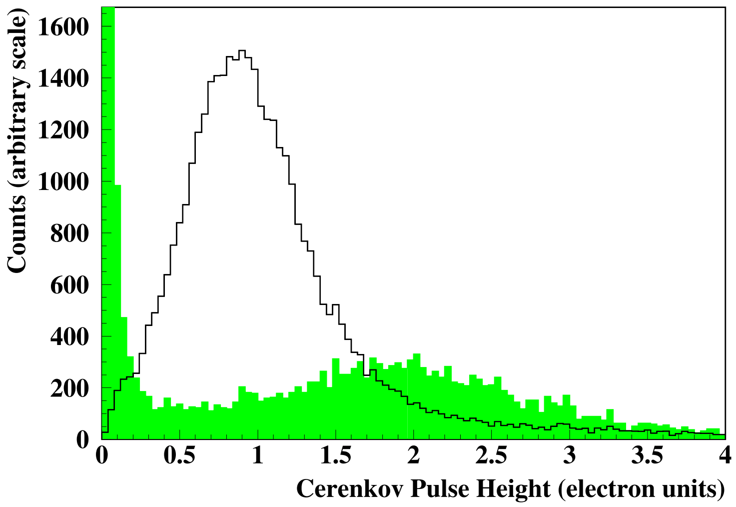

Figure 6.6: Pulse height spectra (in electron units) from the Čerenkov counter for electrons (open histogram) and photons (shaded histogram).

Table 6.3: Fraction of γ candidates which appear as "conversions", having pulse heights of 1.5 to 3.0 MIPS in both $H2$ and Č.

Resonance region	γ candidates	"Conv." (all)	"Conv." as % of total	"Conv." retained after $H1 \cdot H2'$ cut	Conv. lost as % of total
η_c	5086	380	7.5 ± 1.3	370	0.20 ± 0.06
${}^1P_1$	26238	2004	7.6 ± 0.6	1870	0.51 ± 0.04
η_c'	26940	2250	8.4 ± 0.5	2093	0.58 ± 0.05